Production and application of low-energy, high-current electron beams

G.E. OZUR, D.I. PROSKUROVSKY, V.P. ROTSHTEIN, AND A.B. MARKOV

Institute of High Current Electronics, Tomsk, Russia

Abstract

This article reviews experiments on the production of low-energy, high-current electron beams (LEHCEB) and their use for surface modification of materials. It is shown that electron guns with a plasma anode and an explosive emission cathode are most promising for the production of this type of beams. The problems related to the initiation of explosive emission and the production and transportation of LEHCEBs in plasma-filled diodes are considered. It has been shown that if the rise time of the accelerating voltage is comparable to or shorter than the time it takes for an ion to fly through the space charge layer, the electric field strength at the cathode and the electron current density in the layer are increased. Experimentally, it has been established that the current of the beam transported in the plasma channel is 1–2 orders of magnitude greater than the critical Pierce current and several times greater than the chaotic current of the anode plasma electrons. Methods for improving the uniformity of the energy density distribution over the beam cross section are described. The nonstationary temperature and stress fields formed in metal targets have been calculated. The features of the structure-phase transformations in the surface layers of materials irradiated with LEHCEBs have been considered. It has been demonstrated that in the surface layers quenched from the liquid state, nonequilibrium structure-phase states are formed. These states, together with the surface smoothing and cleaning, improve some surface-sensitive properties of the irradiated materials, such as the electric strength of metal-electrode vacuum gaps, the fatigue properties of titanium alloys, and the wear resistance of cutting tools made of high-speed steels and hard alloys. It has also been demonstrated that the pulsed melting of film–substrate systems makes it possible to execute efficient surface alloying. A description of an LEHCEB source with a plasma anode based on a high-current reflected discharge is given and the results of its testing and application are presented.

Keywords: Double layer; Electron-beam irradiation; High current electron beams; Plasma-filled diodes; Surface modification of materials

1. INTRODUCTION

The generators of wide-aperture ($S > 10$ cm^2) low-energy (20–40 keV), high-current (10–30 kA) electron beams (LEHCEBs) of microsecond duration are of considerable interest primarily as candidates for surface treatment of materials (Proskurovsky *et al.*, 1996, 1998). Other fields of possible use of LEHCEBs are the production of high-power X-radiation pulses with a photon energy of 1–10 keV and physics of high energy densities in matter.

The most promising systems for the production of LEHCEBs are electron guns with a plasma anode and an explosive-emission cathode (Nazarov *et al.*, 1994, 1997). Plasma-filled diodes (PFDs) are more advantageous than vacuum diodes in almost all characteristics such as the emissive properties of the cathode and its lifetime, the current density in the acceleration gap, the magnitude of the transportable current, the length of the transportation channel, and the cross-sectional uniformity of the electron flow. The development of an additional system for the formation and power supply of a plasma anode is not a complicated engineering problem and, in view of the mentioned advantages, is quite rewarding.

This article considers the principle of formation of a high-current electron beam in a PFD (Section 2) and some physical aspects of the formation of a plasma anode (Section 3), excitation of explosive emission at the cathode of a PFD (Section 4), and formation (Section 5) and transportation (Section 6) of a magnetized LEHCEB in a plasma channel. Some data are reported on the limitations of the beam pulse duration in plasma-filled systems (breakdown transverse to

Address correspondence and reprint requests to: G.E. Ozur, High Current Electronics Institute, 4 Akademichesky Ave., 634055 Tomsk, Russia. E-mail: ozur@lve.hcei.tsc.ru

the guide magnetic field lines, excitation of a plasma-beam discharge). The factors that determine the cross-sectional uniformity of the electron flow are considered. Section 7 presents the results of calculations of the nonstationary temperature and stress fields that are induced in a metal target. Features of the nonequilibrium structure-phase transformations realized on pulsed melting are also considered. Examples of the use of LEHCEBs for improving some material properties (the electric strength of the vacuum insulation, the resistance to wear, fatigue strength, etc.) are given. In Section 8, an LEHCEB source with a plasma anode based on a reflected discharge is described, which is used for the modification of the surface layers of various materials, and some data obtained in operating this system are reported.

2. THE PRINCIPLE OF PRODUCTION OF HIGH-CURRENT ELECTRON BEAMS IN PLASMA-FILLED DIODES

The idea to produce high-current electron beams in plasma-filled systems goes back to the works of Plyutto *et al.* (1969) performed in the 1960s. In the 1970s, Iremashvili *et al.* (1975) embodied this idea in high-current electron guns "with a cold cathode and a plasma anode." A considerable contribution to the understanding of the processes involved in the generation of high-current electron beams in plasma-filled systems was the study of high-current "direct discharges" that was carried out in the 1970–1980s by researchers of the Kharkov Physicotechnical Institute (Lutsenko *et al.*, 1976, 1988). All these studies have made it possible to reveal the principal features of the behavior of plasmas with a particle density of 10^{11}–10^{14} cm^{-3} in the strong pulsed electric fields and demonstrate the dominant role of the double space charge layers appearing in plasmas in the production of high-current electron beams.

In general, the mechanism for the generation of an electron beam in a PFD is as follows. The acceleration gap and the beam drift space are preliminarily filled with plasma of moderate density (10^{12}–10^{13} cm^{-3}). The plasma column can be produced either by injecting plasma from point generators (e.g., spark generators, Fig. 1a) or by bulk ionization of the working gas in a high current reflected discharge (Fig. 1b). Owing to its high conductivity, the plasma has a potential close to the ground (anode) potential. Once the plasma column has been formed, an accelerating pulsed voltage is applied to the cathode of the electron gun. The electric field is localized within the cathode layer of ion space charge, whose thickness is generally much less than the cathode–anode gap spacing. As a result, the electric field at the cathode, E_κ, reaches a high value (generally, no less than 100 kV/cm), and explosive electron emission is initiated at the cathode, resulting in the formation of dense plasma blobs that constitute an electron emitter. After a time (generally, about 100 ns), these individual cathode plasma blobs merge to form a solid emitting surface. Once explosive emission has been initiated, the accelerating voltage is lo-
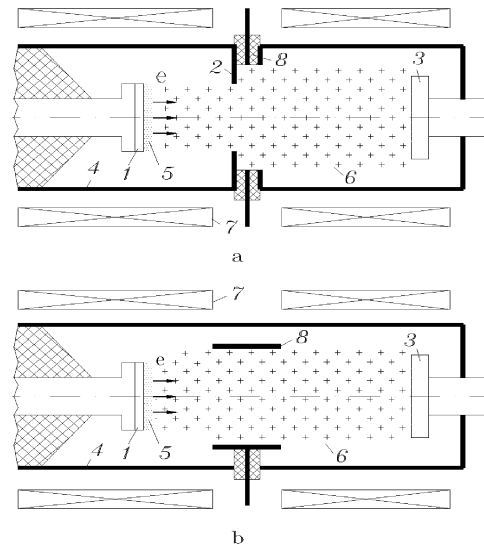
Fig. 1. Schematic diagrams of high-current diodes with a plasma anode based on spark plasma generators (a) and a high current reflected discharge (b). 1: explosive-emission cathode; 2: diaphragm; 3: collector; 4: case; 5: cathode plasma; 6: anode plasma; 7: solenoid; 8: spark plasma generator (a) and anode of reflected-discharge (b).

calized within the double layer (DL) between the cathode and anode plasmas that carries a bipolar flow of charged particles.

The electron and ion current densities in the DL (we assume it to be one-dimensional) are generally related by the classical Langmuir formula

$$J_e = J_i (M/m)^{1/2} = 1.85 \times 2.33 \times 10^{-6} V^{3/2}/d^2, \quad (1)$$

where M and m are the ion and the electron mass, respectively, V is the fall voltage across the layer, and d is the layer thickness. The ion current density in turn is the sum of two components: the Bohm term and the drift term, which is determined by the velocity of the mutual motion of the cathode and anode plasmas (including the layer expansion velocity), v_d:

$$J_i = 0.4 e n_a (2kT_e/M)^{1/2} + e n_a v_d. \quad (2)$$

Here, n_a and T_e are the anode plasma density and temperature, respectively, k is Boltzmann's constant, and e is the electron charge.

The electron beam accelerated in the DL is transported through the anode plasma to a collector, which can serve as a support for samples and articles to be treated. To prevent the beam from pinching, an external guide magnetic field is used. In the case where a plasma anode is formed with the help of a reflected discharge, the guide magnetic field plays one more role, providing the initiation and operation of the discharge.

3. FORMATION OF A PLASMA ANODE

There are two methods generally used for the creation of the column of plasma filling the acceleration gap and the drift space. The first method is based on the use of the plasma of vacuum sparks (arcs) that issues from the region of its generation into the fill space. The small dimensions of the spark and arc gaps allow one to consider them point plasma sources. There exist a variety of designs of this type of plasma source: Bostik end-face guns, coaxial plasma guns, capillary-type plasma guns, and so forth.

The second method is to realize bulk ionization of the working (or residual) gas with the help of an auxiliary hot-cathode gun (Lutsenko *et al.*, 1976; Krastelev *et al.*, 2000) or by initiating a gas discharge of high ionizing ability, for example, a high-current reflected (Penning's) discharge (RD; Nazarov *et al.*, 1997). If the rate at which the plasma column loses ions is less than or of the order of the ion production rate, a rather high degree of ionization of the working gas and, hence, a correspondingly high plasma density can be achieved. For instance, in the experiments described in Lutsenko *et al.* (1976, 1988), the plasma density could be varied in the range 10^{12}–10^{13} cm^{-3} and the ionization degree approached 100%. However, auxiliary electron guns are inefficient to employ because they add complexity to the system design and, moreover, hot cathodes used in them have short lifetimes. Therefore, high-current reflected discharges are more promising as a means for creating the plasma anode.

In this connection, an important note should be made. It is generally believed (Kreindel, 1977) that the high-current (i.e., arc) reflected discharge is unsuitable for producing a stable plasma column with an appropriately uniform density distribution because of the chaotic behavior of cathode spots. Broadly speaking, this doubt is reasonable. However, our experience in developing electron guns with a plasma anode based on a high-current RD has shown that they are capable of producing electron beams with a quite acceptable cross-sectional energy density distribution (beam autographs do not show pronounced microirregularities).

It should also be noted that the high-current RD has not been adequately investigated since it was not considered a candidate for use in charged particle beam sources. An exception was the work of Arzhannikov *et al.* (1978, 1984), who utilized this type of discharge to create a long (240 cm) plasma column in experiments on studying the processes involved in the transportation and relaxation of high-power relativistic electron beams. Rather uniform radial plasma density distributions have been obtained for plasma columns produced at comparatively high pressures of the working gas (hydrogen, 0.01–0.1 Torr) for a magnetic field strength of 25 kOe and currents of up to 60 kA. The degree of gas ionization approached 100%.

Below we discuss the principal results of our experiments on the production of plasma anodes with the use of a set of arc plasma sources and with the help of a high-current reflected discharge.

3.1. Production of a plasma anode with the use of arc plasma sources

The probe method was used to investigate the saturation ion current density distribution and other parameters of the plasma anode produced by 12 spark (arc) sources arranged in a circle around the hole in the anode electrode (Fig. 1a; Nazarov *et al.*, 1994; Ozur & Proskurovsky, 1989, 1990). The circle (plasma anode) diameter was 3.4 or 7 cm. Structurally the plasma sources were TVO resistors with grinded-off end faces. The cathodes were the (graphite) inner conductors of the resistors. The arc ignition in the plasma generators was realized by initiating breakdown over the surface of the ceramic envelope of a resistor. The current amplitude was varied in the range 0.4–4 kA and its duration in the range 2–5 μs. The resistive decoupling of the plasma sources ensured their stable simultaneous operation beginning from a voltage of 6–7 kV. A set of four Langmuir probes arranged in a line at different radial positions was placed behind a diaphragm and could be displaced along the system axis without deterioration of vacuum. Probe signals were recorded with an oscilloscope with a bandwidth of 50 MHz.

The principal measurement results are as follows:

1. The plasma density increases approximately linearly with current and agrees in value with its estimates by the erosion rate of the cathode material (carbon) of the plasma generators. As the distance between the probe and the plane of location of the plasma sources, l_{a-p}, increases, the plasma density decreases as $(l_{a-p})^{-1}$.
2. The ion current density and its radial profile may be varied by varying the diameter of a diaphragm mounted on the anode holder (Fig. 2).
3. The pulse-to-pulse reproducibility of the probe signals made up about 20%, which is quite acceptable.
4. The velocity of expansion of the anode plasma along and transverse to the magnetic field lines was (5–10) $\times 10^4$ and (1–2) $\times 10^4$ m/s, respectively. These high
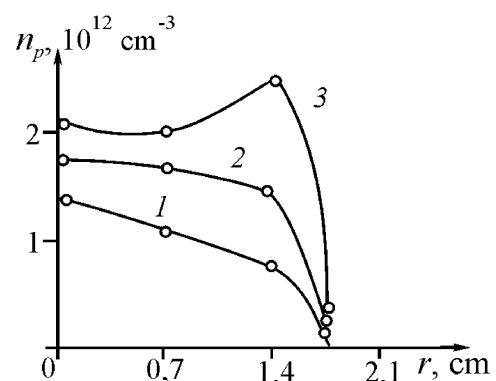
Fig. 2. Typical anode plasma density distributions for different values of the diaphragm hole: 2 (*1*), 2.7 (*2*), and 3.4 cm (*3*), respectively. $H = 2$ kOe, $l_{a-p} = 3$ cm.

velocity values are due to the pressure of the self magnetic field of the current flowing in the spark plasma sources, that is, these sources are, in fact, end-face-type plasma guns. As follows from (1) and (2), for high velocities of the plasma motion in the axial direction, one should choose the lower values of the plasma density; otherwise, the plasma current, given by $I = J_i (M/m)^{1/2} S$, may appear to be greater than the current of the generator powering the electron gun.

5. The electron temperature determined by the floating potential was 2–3 eV, which is in a good agreement with the data available in the literature.

Thus, it has been shown that there exists a conceptual possibility to create a quasi-uniform plasma column by injecting plasma in the transverse direction. Similar plasma density values and $J_i(r)$ profiles have been obtained for the plasma anode diameter equal to 7 cm (of course, at a higher current).

3.2. Production of a plasma anode by bulk ionization

The use of the plasma of vacuum arcs in LEHCEB sources is quite reasonable for the treatment of widely used metal articles and tools. In special cases, for instance, when treating the surfaces of the electrodes of accelerator tubes, slow-down electrodynamic systems of microwave devices, and medical articles, not only is oil-free evacuation needed, but it is also required to prevent the surface under treatment from being contaminated with the cathode and anode erosion products. Arc (spark) anode plasma sources are one of the major contributors of contaminants. Another disadvantage of the arc plasma sources is the very great energy going for plasma production, since their current makes up 10–20% of the beam current, while to form a beam in DL, only the ion component of the anode plasma current is used which makes up only ≈5% of the total current of the arc sources. Finally, the use of arc plasma sources for the production of a long plasma anode is inefficient for structural reasons.

To overcome these disadvantages, we pioneered the production of a plasma anode with the use of a low-pressure (0.1–1 mTorr) high-current reflected discharge (Proskurovsky *et al.*, 1996; Nazarov *et al.*, 1997). The reflected discharge cathodes (Fig. 1b) are the (grounded) beam collector and the explosive-emission cathode of an electron gun. The cathode is grounded through the decoupling inductor of a voltage pulse generator (VPG). Since the pulse duration of the discharge current was much longer than that of the VPG, we could choose the VPG inductance so that the portion of the discharge current that flowed in the circuit of the explosive-emission cathode was not too low. The total discharge current was controlled over the range 4–400 A with the help of a ballast resistor connected in series with the anode.

Once a pulsed voltage is applied to the anode (Fig. 3), the discharge goes through two main stages: the low-current
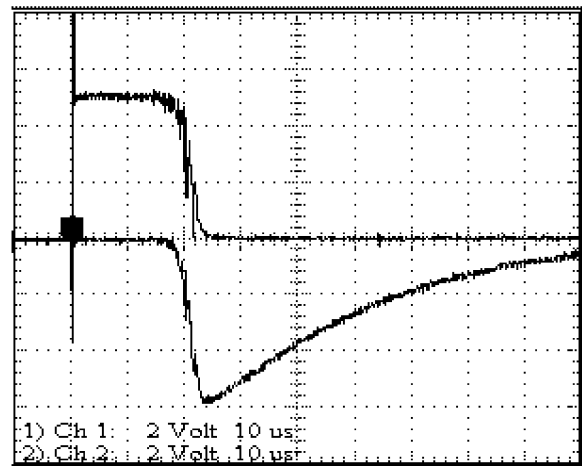
Fig. 3. Waveforms of the voltage in the discharge power supply circuit (upper trace, 2 kV/div) and the discharge current (lower trace, 46 A/div). A Rogowski coil was used as a current gauge. The signal is inverted. Argon pressure = 0.5 mTorr. $H = 450$ Oe.

(high-voltage) stage and the high-current (low-voltage) stage. The low-current stage of RDs has been investigated rather well, although mainly for dc discharges (Babertsyan *et al.*, 2000). As for the high-current stage, it, as mentioned, has been studied inadequately; therefore, we have performed a series of experiments to elucidate the processes involved in this stage of RD discharges.

The principal results of our investigations are as follows:

1. For the mentioned range of working gas (argon) pressures, the RD current in the high-current stage shows a very weak dependence on both the gas pressure and the magnetic field strength (in the range from 300 to 4000 Oe). The operating voltage of the discharge is 150–200 V, and it is almost equally distributed among the cathode and anode space charge layers. The electron temperature, estimated from the probe characteristic, lies in the range 5–7 eV, which is typical of low-pressure discharges.

2. An increase in discharge current leads to an (substantially slower) increase in the density of the ion current onto the cathodes. For instance, as the discharge current was increased from 4 to 300 A, the ion current density increased only five times (from 0.03 to 0.15 A/cm^2). This result suggests that the current of an arc RD is carried in the main by the cathode spots. Photography of the discharge glow has shown that the number of cathode spots is roughly proportional to the current.

3. The rise time of the discharge current, as the discharge goes into the high-current stage, is in about inverse proportion to the gas pressure.

4. The threshold gas pressure at which the RD is still able to go into its high-current stage decreases with increasing anode area.

5. The delay times for the transition of an RD into the high-current stage have a small (not over 6–8%) pulse-to-pulse spread. These times are less than those estimated by the well-known formula (Expression 4) for the glow-to-arc transition by 1–2 orders of magnitude. The mechanism for this transition is related to the formation of cathode spots due to the charging of the cathode dielectric inclusions and films by the ion current that is followed by their breakdown (Lutz, 1974). Actually, the ion current density that we measured in the high-voltage stage of a discharge was about 1 mA/cm^2, which should give a transition time of the order of 1 ms, whereas these times are actually no longer than 20–40 μs.

6. The transition times did not depend on the method of evacuation (oil or oil-free vacuum), but were determined in the main by the state of the near-surface layer of the collector. For instance, as the collector was exposed to 10 pulses of an electron beam with an energy density of 10 J/cm^2, the transition time increased about twofold for oil-free vacuum.

7. Plasma was detected in the space between the anode and the electron gun wall, which formed a system of the "inverted magnetron" type. Although the density of this plasma is 4–5 times lower than that in the main discharge column, it may substantially influence the operation of the electron gun (Karlik *et al.*, 2002).

4. EXCITATION OF EXPLOSIVE EMISSION AT THE CATHODE OF A PLASMA-FILLED DIODE

The excitation of explosive emission in a PFD is substantially different from that in a vacuum diode. For a PFD, the electric field E_κ depends not only on the applied voltage and electrode geometry, but also on the rise time of the pulsed accelerating voltage, τ_{rt}: the shorter τ_{rt}, the higher E_κ. The difference in E_κ values between the case of an accelerating voltage with a long rise time ($\tau_{rt} \gg \tau_f$, τ_f is the characteristic time it takes for an ion to fly through the cathode layer of space charge) and the case of a stepped accelerating voltage ($\tau_{rt} = 0$) may be very significant. An estimation of this difference can be performed from the relation

$$E_1/E_2 = (eV/W_i)^{1/4}, \qquad (3)$$

where E_1 and E_2 are the values of E_κ for $\tau_{rt} \ll \tau_f$ and $\tau_{rt} \gg \tau_f$, respectively, V is the accelerating voltage, and W_i is the kinetic energy of the anode plasma ion at the entrance into the layer.

For the case $\tau_{rt} \approx \tau_f$, the system of equations for the layer should be solved by numerical methods, and this was done by Kreindel' *et al.* (1991). As expected, for this case, the values of E_κ lie in the range between the limiting values E_1 and E_2. Typical calculated waveforms of $E_\kappa(t)$ are given in Figure 4. The calculation results are in satisfactory agreement (to within 30%) with the data of an experiment on measuring the dependence of the probability of appearance of an explosive emission center on the electric field for a pulsed voltage of nanosecond (40 ns) duration.

Another important distinguishing feature of PFDs compared to vacuum diodes is the ion bombardment of the cathode that stimulates the formation of explosive emission centers through the charging and breakdown of nonmetal inclusions and films (Lutz, 1974). Experience shows that the latter circumstance provides for a better uniformity of explosive emission over large-area cathodes, the opportunity of operation at lower (2–5 times) E_κ, and substantially longer lifetimes of cathodes (Nazarov *et al.*, 1994).

However, the experimentally observed almost inertialess operation of the cathode (with a time lag in general not over 10 ns) in a PFD has not yet been explained adequately. Actually, in our experiments, the density of the ion current onto the cathode were typically $J_i \approx 1$ A/cm^2; that is, the breakdown delay times t_3 should be about 1 μs, in accordance with the well-known relation (Pfeil & Griffiths, 1959)

$$j_i t_3 = \varepsilon\varepsilon_0 E_{br}, \qquad (4)$$
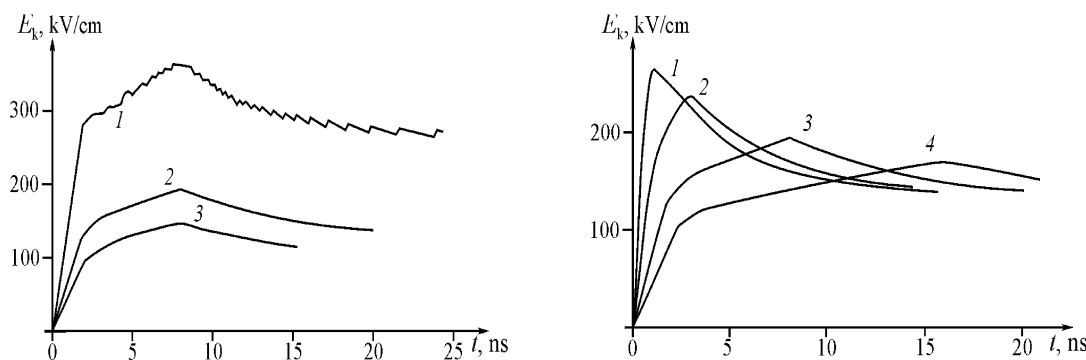
Fig. 4. The electric field at the cathode calculated for different values of the plasma density (a): 5×10^{12} (*1*), 10^{12} (*2*), and 5×10^{11} cm^{-3} (*3*) (for $\tau_{rt} = 8$ ns) and for different values of τ_{rt} (b): 1 (*1*), 4 (*2*), 8 (*3*), and 16 ns (*4*) (for $n_a. = 10^{12}$ cm^{-3}). Ion species: C$^+$; peak voltage = 20 kV.

where ε and E_{br} are, respectively, the dielectric permitivity and the breakdown electric field for the film material.

## 5. GENERATION OF AN ELECTRON BEAM IN A PLASMA-FILLED DIODE

As mentioned in Section 2, the current density of an LEHCEB is specified, first of all, by the ion current density of the anode plasma. Departures from the value determined by relation (1) appear during a rapid rise of the voltage across the DL, for instance, within the voltage pulse rise time. If the ions, because of their inertia, do not manage to react to a change in the field in the DL, the layer thickness may be substantially smaller than that in the steady-state case. It follows that J_e may substantially exceed (for a time) the Langmuir limit (Kreindel' *et al.*, 1991). The limiting value of the electron current density that is achieved for a voltage pulse with a perfect leading edge ($\tau_{rt} = 0$) is determined from the relation obtained by Kreindel' *et al.* (1991):

$$J_e = en_a(eV/2m)^{1/2}. \quad (5)$$

Typical waveforms of the electron current density calculated for different values of τ_{rt} are given in Figure 5. The calculation results are in satisfactory agreement with experimental data both in the shape of waveforms and in magnitudes of the current density.

These results suggest that during the non-steady-state stage the current density in the DL, for a certain time (of the order of several times of flight of the ion through the DL), may substantially exceed the Langmuir limit. This is due to the lesser thickness of the non-steady-state layer and the greater degree of neutralization of the electron space charge in the layer. Thereafter, the thickness of the DL increases and the ion space charge distribution and the electron current density approach the value determined by relation (1).

Relation (1) also indicates that the distribution of the LEHCEB current density over the beam cross section is determined by the density distribution of the ion current from the anode plasma. Of course, this is true if the cathode plasma has a density greater than the anode plasma density.
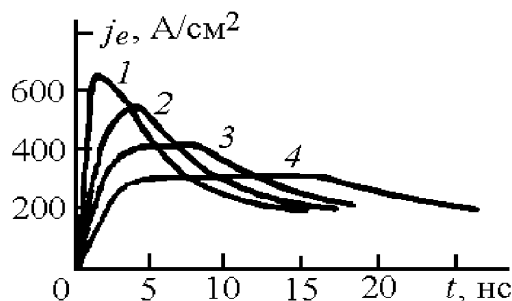
Fig. 5. Waveforms of the current density in the DL calculated for different values of τ_{rt}: 1 (*1*), 3 (*2*), 8 (*3*), and 16 ns (*4*). $n_a = 10^{12}$ cm^{-3}; $V = 20$ kV; ion species: C$^+$.

It follows that to provide a uniform LEHCEB in its cross section, it is necessary to have a uniform plasma anode. Some methods of attack of this problem are discussed in Ozur *et al.* (2000*a,b*).

Analysis of relation (1) allows one more conclusion. With a sufficiently high power of the external power supply circuit (which provides a comparatively slow variation of the voltage across the DL) the DL thickness is established self-consistently in accordance with the density of plasma having a lower emissive power (more often this is the anode plasma). It follows that in PFDs, in contrast to vacuum diodes, there takes place suppression of the development of the so-called leaders—explosive emission centers, having appeared earlier than the other ones, which expand with a higher velocity and, therefore, carry a higher current (Mesyats & Proskurovsky, 1989). As a result, the microirregularities of the electron flow that appear due to the discrete character of the emission from the cathode are suppressed to a large extent even in the beam formation region.

The mechanism for the limitation of the beam pulse duration in a PFD is different for the methods of production of a plasma anode presented in Figure 1. In the gun with a plasma cathode based on arc sources, the breakdown of the diode is due to the plasma appearing at the anode diaphragm edge and at the collector as they are bombarded with the beam electrons (Nazarov *et al.*, 1994). For a plasma cathode based on a high-current reflected discharge, the mechanism of the breakdown of the diode is more complicated. In our opinion, there are two principal reasons for the breakdown: the increase in anode plasma density resulting from the development of a beam-plasma discharge (BPD) and the expansion of the cathode plasma transverse to the lines of force of the magnetic field as a consequence of the centrifugal instability developing in the cathode plasma, as observed in magnetically insulated vacuum diodes (Bugaev *et al.*, 1982).

As to the development of the BPD, it is supported by the following data. As follow from our probe measurements, the degree of ionization of the working gas for the investigated ranges of discharge currents and working gas pressures is not over 20–30% (Nazarov *et al.*, 1997). Hence, the stored neutrals, as they are ionized, are capable of providing a considerable increase in current in the DL. In our case, the criterion for BPD ignition (Lebedev *et al.*, 1976) is readily fulfilled, and the estimates of the rate of ionization of neutrals in the BPD give, in the end, the rate of current rise observed in experiment (typical waveforms are given in Fig. 6).

The fact that breakdown occurred transverse to the magnetic field lines is supported by the traces of intense erosion on the wall of the electron gun that lie roughly in the plane of the cathode emitting surface. The breakdown in the radial direction is enhanced by the plasma presence in the space behind the anode (in radius, Section 3.2). An increase in internal diameter of the case (which is equivalent to an increase in cathode–wall gap spacing) leads to a certain
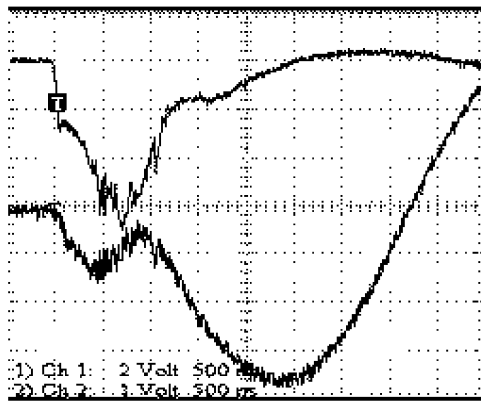
Fig. 6. Typical waveforms of the accelerating voltage (upper trace, 10.5 kV/div) and the total cathode current (lower trace, 15 kA/div). $H =$ 2 kOe; generator charge voltage = 30 kV; argon pressure = 0.6 mTorr. Diameter of the cathode emitting surface = 6 cm.
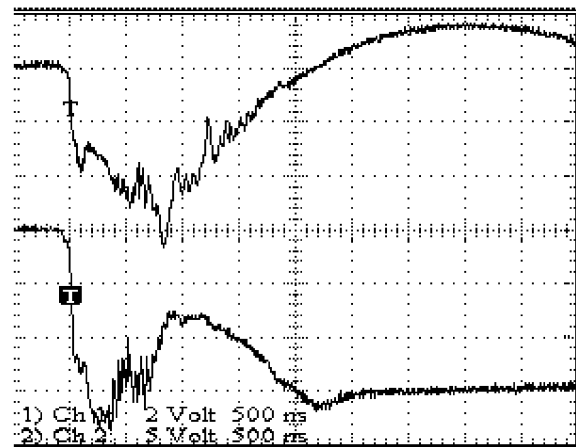
Fig. 7. Typical waveforms of the accelerating voltage (upper trace, 10.5 kV/div) and the beam current onto the collector (lower trace, 6.3 kA/div). $H = 2$ kOe; generator charge voltage = 28 kV; argon pressure in the transportation channel: 0.6 mTorr. Diameter of the cathode emitting surface: 6 cm.

increase in pulse duration. For instance, for diameters of 15.8 and 20.9 cm at an argon pressure of 0.5 mTorr, the average pulse durations were 2.3 and 3 μs, respectively.

6. TRANSPORTATION OF AN LEHCEB IN A PLASMA CHANNEL

The transportation of a beam for considerable distances (10 cm and more) makes it possible to solve some problems. First, it becomes possible to additionally smooth over the beam microirregularities associated with the discrete character of the electron emission from the cathode (especially, early in the pulse). Second, the beam energy at the collector can be changed by varying the beam transportation length (Nazarov *et al.*, 1994). Third, placing the collector at a longer distance from the acceleration gap allows one to avoid purely structural complications if the articles under treatment need to be moved and rotated in the irradiation zone.

When a magnetized LEHCEB is transported in plasma under the conditions of complete charge neutralization, one must, however, take into account the possibility of growth of aperiodic (Pierce and beam-drift) instabilities that lead to the appearance of a virtual cathode in the beam and to a limitation of the beam current (Nezlin, 1982). Nevertheless, our experiments have shown that the transportation of an LEHCEB with a current exceeded the thresholds of these instabilities by 1–2 orders of magnitude is realizable, and this is illustrated by the waveforms given in Figure 7. It can be seen that the beam current reaches 20 kA as early as within 250–300 ns after the beginning of the pulse with the Pierce current equal to only 160 A for the given electron energy (20 keV). Taking into account the final value of the guide magnetic field, according to Ignatov and Rukhadze (1984), increases the calculated Pierce current no more than 2–3 times. Hence, this substantial (30–50-fold) excess of the beam current over the Pierce current is due to the corre-

sponding excess of the plasma density in the transportation channel over the beam electron density, that is, due to the "plasma stabilization" of the beam (Nezlin, 1982). It is not improbable that some overcompensation of the beam space charge also plays some part, and this abruptly increases the Pierce current (Vybornov *et al.*, 1988).

Simple estimates also show that the beam current onto the collector is greater than the chaotic electron current from the anode plasma, $I_{ea} = en_a(8kT_e/\pi m)^{1/2}S/4$, by about an order of magnitude. This argues against the statement (Nezlin, 1982) that this current is the threshold current that still may propagate through the plasma without a virtual cathode forming in the plasma. In this case, it is implied that the appearance of a virtual cathode limits the beam current at a level not exceeding the chaotic current of the plasma electrons. A considerable portion of the excess of the beam current over I_{ea} that we observed in our experiments is associated with the drift term in (2) (which was absent in the conditions of Nezlin, 1982), while the other portion is due to the non-steady state of the DL at the early stage of beam formation ($t < 500$ ns).

In our experiments, a noticeable decrease in beam current compared to the injection current was observed only for rather long transportation channels ($l_{ch} = 20$–50 cm). The decrease in beam current and energy density with increasing l_{ch} was gradual (Fig. 8). In our opinion, a virtual cathode appeared in the channel, but its potential, established self-consistently, was such that a considerable portion of the beam passed to the collector due to the spread in longitudinal velocities of the electrons.

Another phenomenon that limits the beam energy is the relaxation of its kinetic energy due to the collective interaction of the beam electrons with plasma. The energy transferred from the beam to the plasma may go into heating the plasma, excitation of microwave oscillations, and accelera-
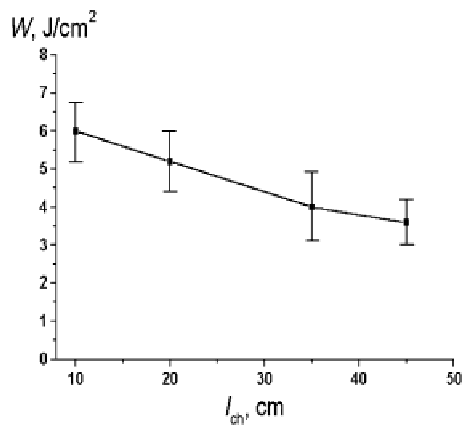
Fig. 8. The beam energy density at the collector as a function of the transportation channel length. $H = 2$ kOe, generator charge voltage = 28 kV; argon pressure in the transportation channel: 0.4 mTorr. Diameter of the cathode emitting surface: 6 cm.

tion of the plasma ions (Lutsenko *et al.*, 1976; Nezlin, 1982). However, for microsecond LEHCEBs, the percentage of the beam energy lost in the plasma has appeared, in the average, relatively small (10–15%), and these losses are observed in the main early (<1 μs) in the pulse (Nazarov *et al.*, 1995).

In the course of transportation of an LEHCEB, not only are a decrease in current with increasing drift channel length and the losses of the beam kinetic energy possible, but also the radial current (energy) density distribution may transform.

For instance, an increase in beam energy density in the near-axis region (Fig. 9, curve 1) was observed by Nazarov *et al.* (1996) for a beam transported in a system with a plasma anode based on arc plasma sources. This "focusing" of the electron beam was due to the accumulation of ions in
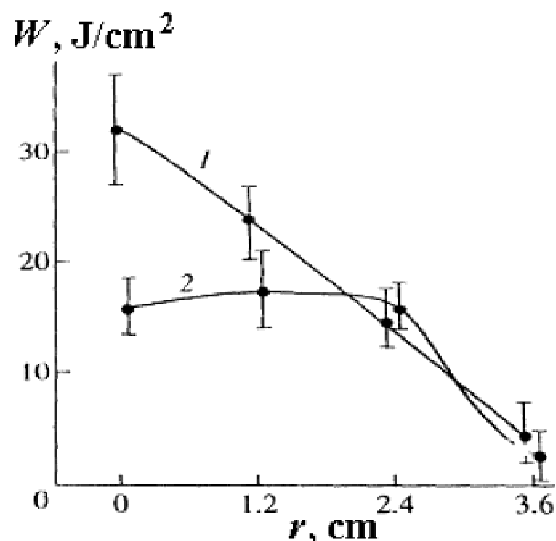
the near-axis region of the beam drift channel, resulting from the radial electric field present in the beam. The appearance of this field was related to the fact that the anode plasma density in this system was comparable to the beam electron density and, near the collector, could be even lower than this quantity, since n_a is in roughly inverse proportion to the anode–collector distance. To compensate this effect, the plane cathode has been replaced with a hollow one to reduce the density of the injected beam in the near-axis region. As a result, the radial distribution of the energy density became more uniform (Fig. 9, curve 2).
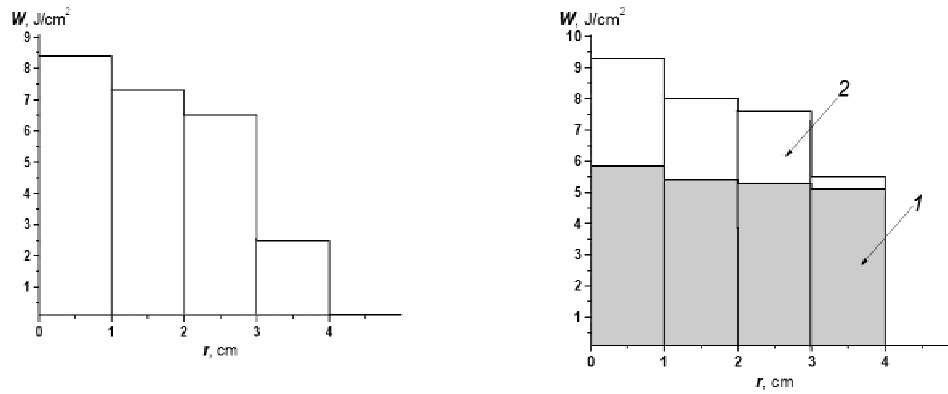
A system with a plasma anode based on a high-current reflected discharge allows one to preclude the above beam focusing owing to an increased (generally 3–5 times) density of the anode plasma and its uniform distribution along the beam axis. As a result, the plasma density exceeds the beam electron density throughout the drift channel and the beam space charge appears to be completely neutralized. Thus, the energy distribution over the beam cross section is specified by the initial distribution of the plasma density in the discharge column.

Experiments on controlling the beam radial profile are described in Ozur *et al.* (2000a, 2000b). Since a high current reflected discharge operates with cathode spots, the distribution of the latter over the cathode surface substantially affects the radial profile $n_a(r)$. With the help of probe measurements of the ion current density and photographing the discharge glow, it has been established that an increase in discharge current increases the number of cathode spots in the peripheral (in radius) discharge region and, as a consequence, improves the uniformity of the distribution $n_a(r)$. This has the result that the energy density distribution over the beam cross section becomes more uniform as well (Fig. 10).

The increase in number of cathode spots in the discharge peripheral region can be explained in a rather simple way. Since cathode spots are sources of intense electron emission, their operation is governed by the closing of the electron current onto the anode. Obviously, the spots operating at a radial distance close to the anode radius are, from this point of view, in a more profitable situation (Nazarov *et al.*, 1997).

7. APPLICATIONS OF LEHCEBs FOR SURFACE TREATMENT OF MATERIALS

Metallic alloys of commercial use are known to show a special combination of physicochemical properties. This cannot be generally attained by conventional metallurgical methods since some requirements contradict one another. For instance, to achieve high strength, it is necessary to form second-phase disperse particles in the material bulk that retard the motion of dislocations. However, the presence of dispersed particles on the surface leads to the development of pitting corrosion. This problem can be resolved for many applications by deposition of type TiN coatings using PVD

Fig. 9. Typical radial distributions of the beam energy obtained for different cathode geometries: *1*: plane cathode; *2*: hollow cathode. $H_z = 4.5$ kOe.

Fig. 10. Cross-sectional beam energy density distribution for different values of the reflected discharge current: 80 (a) and 150 A (b). For case b, the distribution is given for two values of the beam transportation channel length: $l = 12$ cm (*1*) and 22 cm (*2*). $H = 2$ kOe, $p = 6 \times 10^{-4}$ Torr.

and CVD processes. This approach, however, has some limitations. For instance, as for medical implants and surgical instruments, there is a risk of delamination of the TiN coating, which is associated with the presence of a coating–substrate interface. Ion implantation is also inapplicable in this case, and this is mainly associated with the small thickness (100–200 nm) of the implanted layer.

The LEHCEB treatment is highly attractive both from the viewpoint of materials science and for applications (Proskurovsky *et al.*, 1997, 1998, 2000). First, the pulsed melting realized in this case makes it possible to dissolve second-phase particles and the superfast quenching from liquid state results in the formation of nonequilibrium structure-phase states in thin surface layers, which gradually go to the matrix. Second, this type of treatment makes it possible to produce highly concentrated surface alloys by pulsed melting of film–substrate systems. Third, the above factors provide for improving some surface-sensitive properties of the material.

### 7.1. Characteristics of the temperature and stress fields

The nonstationary fields of temperatures and thermomechanical stresses that appear as a result of the energy transfer from the beam to the target are the main factors responsible for the structure-phase state and properties of the material. The temperature field is localized in the heat-affected zone, whose thickness, in the case of LEHCEB irradiation, is not greater than a few tens of micrometers. The stress field consists of two components: an elastic or elastic-plastic stress wave, which propagates from the surface into the bulk of the target, and quasi-static stresses, which, in the case of a thick target, are localized in the heat-affected zone. Since it is difficult to measure temperature and stress fields in an irradiated target, they are generally determined theoretically. The temperature can be calculated by solving the heat equation (Ivanov *et al.*, 1993; Markov & Rotshtein, 1997). The

parameters of the elastic stress wave can be found by solving a system of noncoupled equations of thermoelasticity with the assumption that there are no phase transformations in the material on heating (Markov *et al.*, 1999). For a plane stress state, the quasi-static stresses can be calculated by solving the equation of motion for a plate (Boley & Weiner, 1960; Bardenshtein *et al.*, 2000).

Figure 11 presents the temperature at the surface of a Fe target as a function of time for the modes of initial melting (4 J/cm^2) and noticeable evaporation (12 J/cm^2). It can be seen that the rates of heating and cooling reach values of the order of 10^{10}–10^9 K/s, respectively. Figure 12a gives the coordinate of the melt–solid interface as a function of time for the first irradiation mode. It can be seen that the melt thickness is $\cong 1.3$ μm and its lifetime is of the order of the pulse duration. For the evaporation mode, the thickness of the evaporated layer is $\cong 0.4$ μm and the melt thickness increases to $\cong 5$ μm (Fig. 12b). For premelting modes, the stress wave amplitude is not over ~ 1 MPa. The evolution of the quasi-static stresses at different depths is shown in Figure 13. These stresses are compressive in the surface plane and their magnitude is far in excess of the yield limit of iron,
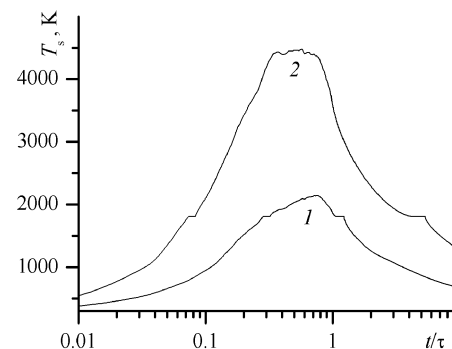
Fig. 11. Time dependence of the surface temperature for iron irradiated in melting (4 J/cm^2, 2.5 μs; *1*) and evaporation (12 J/cm^2, 2.5 μs; *2*) modes, respectively.
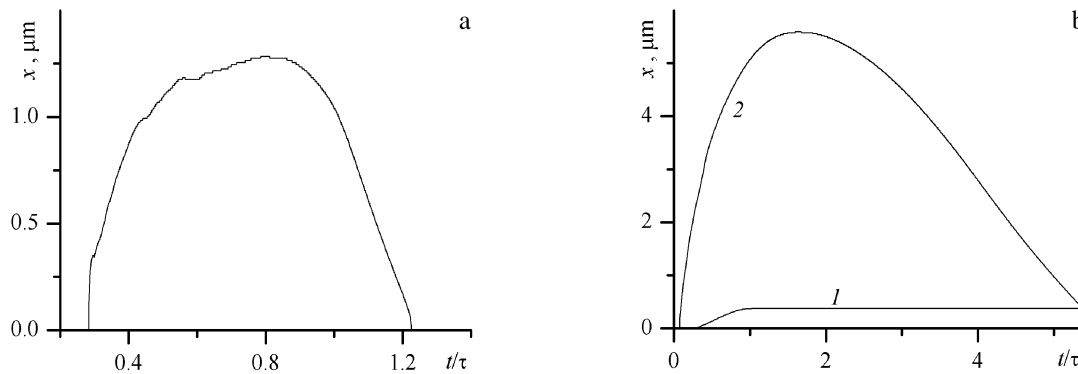
Fig. 12. Time-varying position of the melt front for iron irradiated in the melting (4 J/cm², 2.5 μs) and evaporation (12 J/cm², 2.5 μs) mode (curves *1*, (a) and (b), respectively). Time-varying position of the surface for iron irradiated in the evaporation mode (12 J/cm², 2.5 μs; curve *2*, b).

which is supported in experiment (Dudarev *et al.*, 1996). On complete cooling there are low-intensity (40–80 MPa) residual tensile stresses in the surface layers of the target (Dudarev *et al.*, 1996).

7.2. The effect of pulsed melting on the microstructure and properties of metallic materials

#### 7.2.1. Enhancement of the electric strength of vacuum insulation

It has been demonstrated (Batrakov *et al.*, 1995) that multiply repeated ($N = 20$–50) LEHCEB irradiation of metallic electrodes in the modes of surface melting and evaporation substantially increases the electric strength of the vacuum insulation. This was associated with the cleaning of impurities from the surface layer and by the smoothing of the surface due to melting. To elucidate the origin of the mentioned effects, comparative investigations have been performed (Rotshtein *et al.*, 2002) on the influence of

Fig. 13. Time dependence of the quasi-static stresses at the axe of iron plate 0.4 mm thick irradiated in the premelting mode (2.5 J/cm², 2 μs) at the distances 0 (*1*), 2 (*2*), 5(*3*), 10 (*4*), and 20 μm (*5*) from the surface.

LEHCEB irradiation (20–30 keV, 2.5 μS, 2–12 J/cm²) on the surface morphology, characteristics of crater formation, chemical composition, and microstructure of type AISI 304L and 316L austenitic stainless steels (SS). Samples were made of rod stock (304L and 316L; the irradiated surface was normal to axis of stock) and plate stock (304L; the irradiated surface was parallel to plane of stock). It has been established that the main reason for crater formation is the local overheating followed by explosive ejection of the material at the sites of localization of second phases (Fig. 14a). According to the data of transmission electron microscopy (TEM), the seats of microcraters might be associated with low-melting-point submicron particles of FeS_2. It has been demonstrated that the intensity of cratering for plate stock samples is substantially lower than for rod stock ones. Multiply repeated pulsed melting of SS 304L (plate) and 316L (rod) almost completely suppresses crater formation (Fig. 14b) and reduces the surface roughness compared to the original (on cutting) surface condition.

With the use of Auger electron spectroscopy (AES), it has been established that the surface smoothing is accompanied by removal of O, C, and N impurities from the near-surface layer ($\sim$50 nm). According to TEM data, as a result of fast quenching from liquid state, in the near-surface layer of thickness $\sim$0.5 μm, single-phase (γ-phase) microstructure is formed with a grain size of 0.2–0.6 μm, which is almost two orders of magnitude smaller than that in the original state. The formation of single-phase homogeneous submicron structure with a low density of impurities at intergrain boundaries offers the possibility to considerably enhance the electric strength of vacuum insulation. Figure 15 presents the results of electric strength (first breakdown voltage) tests of vacuum gaps with electrodes of 8 cm diameter (316L, rod) in the original state and after multiply repeated pulsed melting (Proskurovsky, 2002). It can be seen that after irradiation, the electric strength increased by a factor of $\sim$1.8. This is in qualitative agreement with the microstructure evolution.
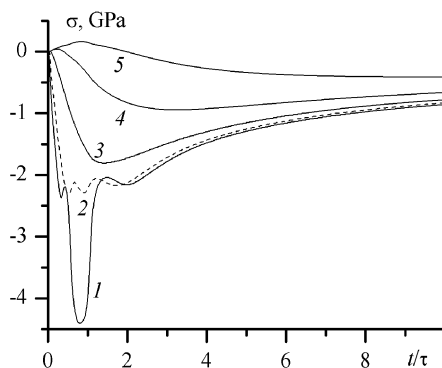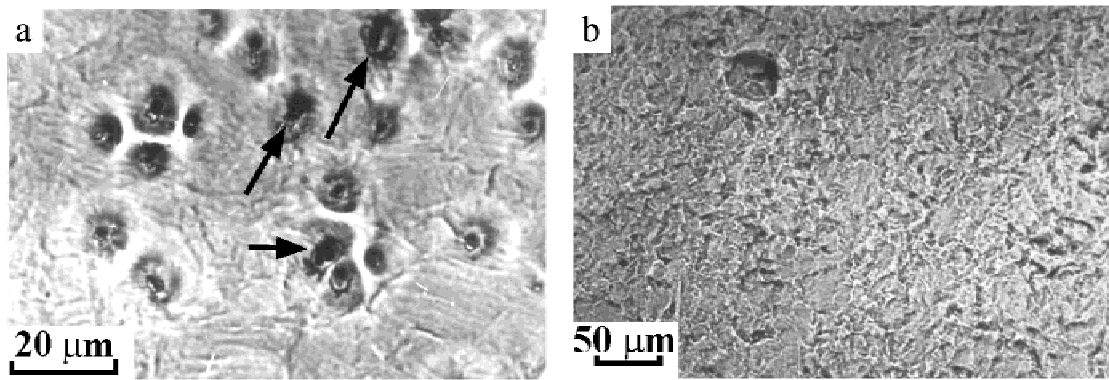
Fig. 14. Optical micrographs of the surface of the SS 304L samples irradiated with LEHCEB: a: rod (~ 3 J/cm^2, 2.5 μs, $N = 1$); b: plate (8 J/cm^2, 2.5 μs, $N = 50$). Microcrater nucleation centers are shown with arrows.

This approach was used to increase the microwave pulse duration generated by a high-power relativistic BWO (Batrakov *et al.*, 2001). It has been shown (Korovin *et al.*, 2000) that the microwave pulse duration in the high-power BWO is limited due to the microwave breakdown occurring in the electrodynamic system. Experiments (Batrakov *et al.*, 2001) have demonstrated that the LEHCEB treatment of the slow-wave structure surface has increased the pulse duration of 3-GW microwaves from 6 to 30 ns.

7.2.2. *Modification of titanium alloys*

In experiments performed with samples of alloys VT8M (Ti-5.8 Al-3.7 Mo) and VT18U (Ti-6.3 Al-4.5 Zr) subjected to preliminary annealing and aging, it has been established (Nochovnaya *et al.*, 1998; Proskurovsky *et al.*, 1998) that

pulse melting cleans oxygen and carbon impurities from the near-surface layers, increases the aluminum content to $\sim 20\%$, makes the distribution of the components in this layer more uniform, and reduces the surface roughness to ~ 0.1 μm. However, in this case, the phase composition changes to some extent, tensile residual stresses of low intensity are formed, and microcraters appear on the surface. When irradiation is performed in optimum modes, cratering can be suppressed. Subsequent annealing recovers the original phase composition and substantially increases the performance properties of the material, such as the fatigue strength (more than by 20%), the endurance (more than 10 times; Fig. 16), the resistance to dust erosion at small loads (more than twice), and the short-term strength (by up to 8%) with a substantially improved plasticity. As this takes place,
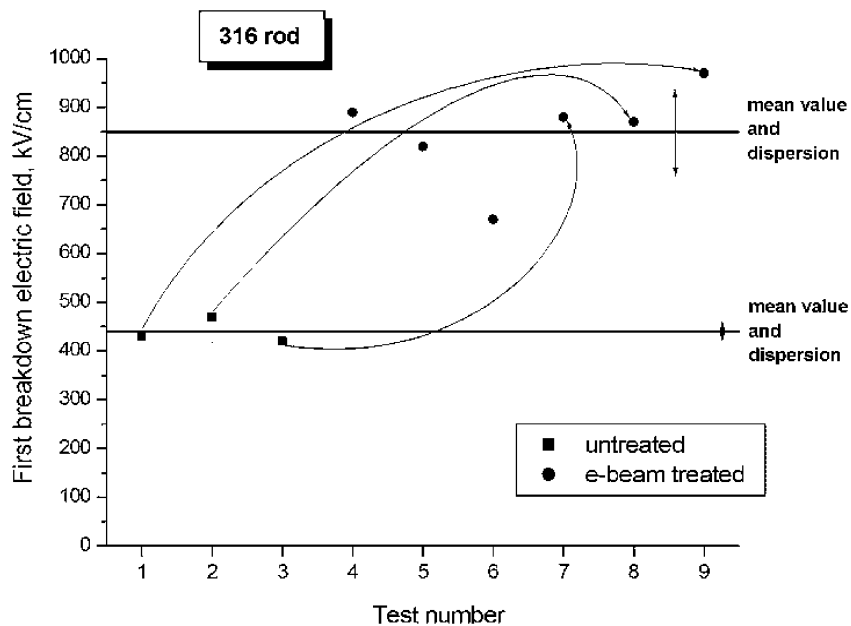
Fig. 15. First breakdown electric field for vacuum gaps with electrodes of 8 cm diameter made of steel 316L (rod) in the original state and after irradiation with LEHCEB (10 J/cm^2, 2.5 μs, $N = 30$).
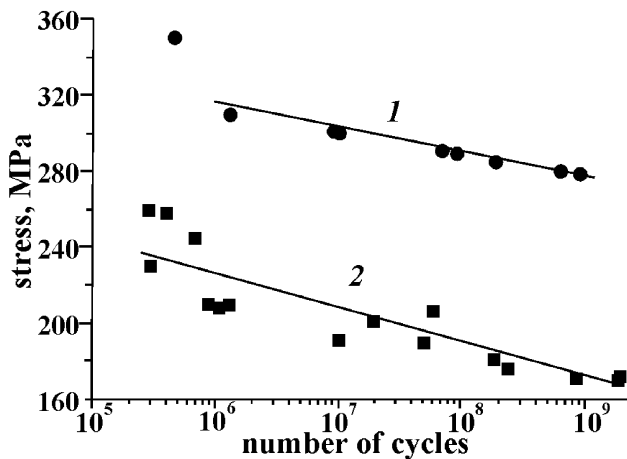
Fig. 16. Fatigue S-N curves for samples made of Ti alloy VT8M in initial state (*1*) and after irradiation (2.5 J/cm², 2.5 μs, N = 40) followed by vacuum annealing (500–550°C, 10 h; *2*).

the surface microhardness and the heat-resistance remain at the original level.

The enhancement of the strength characteristics of the material is related to the smoothing of the surface due to its melting, to its cleaning, and to an increase in aluminum content in the near-surface layer. Fractography performed on static loading has shown that pulsed melting changes the character of fracture from intercrystallite or quasi-viscous to viscous. On cyclic loading, the fracture of untreated samples is initiated at the surface, while typical of irradiated samples is subsurface nucleation of cracks. It is this factor that is responsible for the improvement of fatigue properties of irradiated samples.

7.2.3. Enhancement of the wear resistance of high-speed steels

The structure-phase transformations in the near-surface layers under LEHCEB irradiation have been investigated for preliminary quenched high-speed steel (HSS) S6-5-2 (Fe-0.87 C-6.4 W-5.0 Mo-4.3 Cr-1.9 V, wt.%; Ivanov *et al.*, 2002). The original structure of this steel consists of crystals of lamellar α-martensite and globular particles of type Fe_3M_3C carbide, where M = Mo + W. The melting threshold for the surface corresponds to 3.2 J/cm². Further increasing energy density results in gradual dissolving of the original carbide particles in the near-surface layer. As a result of quenching from liquid state, a structure consisting of α-martensite and residual austenite (γ-phase) is formed, the γ-phase fraction increasing almost linearly with energy density and reaching ~90% at 15 J/cm². If carbide particles are completely dissolved, martensitic transformation is suppressed. At the place of the particles, a structure is formed which consists predominantly of weakly misoriented submicron cells of γ-phase separated by nanosized carbide interlayers. The formation of this cellular structure is related to the fact that, in the process of fast resolidification of the

melt enriched in dissolved impurities (W, Mo, C), these elements are accumulated in the near-surface layer followed by their displacement from the solid solution.

To elucidate the effect of pulsed melting on the wear resistance, cutting tools (drills of 8 mm diameter) were tested in the original state and after irradiation with 7 J/cm² when an abrupt increase in the fraction of M_6C carbide particles was observed. The test results have shown that irradiation reduced the wear of the cutting edge by a factor of ~1.7 compared to unirradiated drills. The enhancement of wear resistance is related to the following changes in microstructure in the surface layer: the fixing of comparatively coarse original carbide particles in the matrix due to their partial liquid-phase dissolving, the formation of new disperse M_3C carbide particles, the increased percentage of the metastable γ-phase and its provable transformation into martensite in the course of cutting, and the formation of residual compressive stresses in the γ-phase.

7.2.4. Enhancement of the wear resistance of hard alloys

It has been shown (Proskurovsky *et al.*, 1998; Ivanov *et al.*, 2000) that irradiation of cutting tools made of hard alloys WC-Co and WC-TiC-Co in the surface melting modes increases the wear resistance of the tools operated at high cutting speeds about threefold. Through the use of TEM, it has been established that this effect is due to the fact that in the near-surface layer, as a result of pulsed melting and fast crystallization, there occurs fragmentation of the cobalt binding and segregation of nanosized particles of new carbide phases in this binding. This substructure shows increased thermal stability in plastic deformation by cutting due to the fact that dislocations are fixed by nanosized second-phase segregates formed in the course of cutting.

An investigation of the action of an LEHCEB on the microstructure, microhardness, and wear resistance of the hard alloy WC-30% Gadtfield steel is described in Gnyusov *et al.* (2002). The binding had the γ-lattice (fcc) and, in contrast to cobalt, featured rather high structural instability in deformation. For irradiation with $E_s \leq 30$ J/cm², irrespective of the number of pulses, the microhardness in the surface layer of thickness up to ~100 μm is observed to increase by a factor of ~1.5 compared to the original state (Fig. 17). Wear tests have shown that the surface hardening is accompanied by a decrease in coefficient of friction by about a half (Fig. 18) and by a substantial increase in wear resistance compared to the original state. It has been demonstrated that pulsed melting has the result that there occurs $\gamma \rightarrow \alpha$-martensitic transformation in the binding phase and the formation of nanosized and submicron carbides W_2C, $M_{12}C$, and $M_{23}C_6$. Similar structure-phase transformations are observed on the wear surface of original samples upon steady-state friction, which is characterized by a minimum wear. It follows that it is these transformations that are responsible for the hardening and enhanced wear resistance of the given material on irradiation.
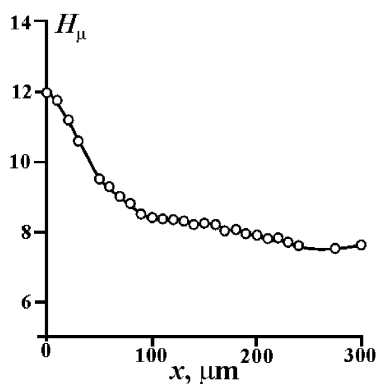
Fig. 17. Microhardness depth profile for hard alloy of WC-30% Gadtfield steel irradiated with LEHCEB (40 J/cm², 2.5 μs, N = 1). The Vickers diamond pyramid load is 1 N.

Experiments (Perry *et al.*, 1999) were performed to investigate the effect of LEHCEB irradiation (2.5 μS, 3–5 J/cm²) on the microstructure and wear resistance of TiN coatings deposited by the PVD method on cutting tools made of the hard alloy WC-TiC-TaC-Co. The upper level of E_s corresponded to initial melting of the coating. The experiments have shown that after irradiation, because of the intense tensile stresses formed at the stage of cooling, microcracks appear in the coating. Notwithstanding this, the coating retains good adherence to the substrate. The stoichiometry and phase constitution of the coating, except for its surface, remain unchanged. In this case, the compressive residual stresses vanish and the concentration of vacancies noticeably decreases, suggesting that pulsed annealing of defects has occurred. These substructural changes increase the wear resistance of TiN-coated cemented carbide inserts almost twofold.

7.2.5. Formation of surface alloys

By surface alloys are implied metastable structures that are formed in the near-surface layers of materials upon ion
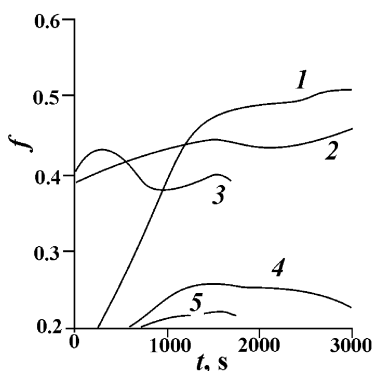
Fig. 18. Friction coefficient versus time for the pin-on-disk system. Pins are made of hard alloy of WC-30% Gadtfield steel: in initial state (*1, 2, 3*); after irradiation (20 J/cm², 2.5 μs, 10 pulses; *4,5*). Disk made of tool steel (HRC 52). Dry friction; normal load 175 H; slide speed (m/s): 0.65 (*1*), 1.4 (*2, 4*), and 2.8 (*3, 5*).

implantation and pulsed melting of film–substrate systems. Ion implantation following pulsed melting is also used (Poate *et al.*, 1983). From the viewpoint of applications, the pulsed melting of film–substrate systems is, in our opinion, of greatest interest since it makes possible the forming of highly concentrated surface alloys whose thickness may be about an order of magnitude greater than that achievable with high-dose ion implantation (Poate *et al.*, 1983). If, because of thermodynamic limitations, the film component content is comparatively low, the mode of nonequilibrium liquid-phase alloying is realized.

In the majority of relevant experiments, nanosecond laser pulses were used (Poate *et al.*, 1983). Because of some circumstances (the comparatively small thickness of the alloyed layer, the small cross-sectional area of the beam, the high coefficient of reflection of the radiation, the low efficiency, etc.), the method of nanosecond laser alloying still remains usable only for investigation of the microstructure evolution. From the practical viewpoint, LEHCEBs seem to be more promising, and this will be demonstrated below.

The features of the nonequilibrium structure-phase transformations taking place in pulsed melting of single-layer (Ta-Fe) and multiplayer (Al-Si and Al-C) film–substrate systems are discussed in Ivanov *et al.* (1994) and Proskurovsky *et al.* (2000). These systems are characterized by limited solvability of the components in the solid state, and the components of the system Al-C are incompatible in the liquid state as well. The experiments have demonstrated the possibility of the formation of metastable phases, including nanocrystalline and amorphous ones. However, the thickness of the modified layer was generally not over ~0.5 μm and was limited, on the one hand, by the thickness of the melt and, on the other hand, by the transition to the evaporation mode in which the bulk of the coating was evaporated. Experimental data demonstrating the possibility of increasing the thickness of the modified layer are presented below.

Figure 19a presents concentration profiles obtained after pulsed melting of a system Ni (3 μm)-Cu. The coating was electroplated. This system is convenient for study since it features unlimited solvability in both the solid and the liquid state. It can be seen that the thickness of the alloyed layer is ~1.5 μm, that is, it is about half the thickness of the original coating. This is associated with the evaporation of some portion of the coating on multiply repeated irradiation. In the surface layer of ~0.5 μm thickness, a single-phase alloy with nearly the same component concentrations is formed. To increase the thickness of the alloyed layer, the operations of coating deposition and pulsed melting were repeated alternately two times. The concentration profiles obtained in this case are given in Figure 19b. It can be seen that, despite the losses associated with the evaporation of the coating, it is possible to form surface alloys with a rather uniform depth distribution of the components and a graded diffusion transition from the alloyed layer to the substrate. In this case, the thickness of the alloyed layer is about an order of magnitude greater than that attainable on nanosecond laser alloying.
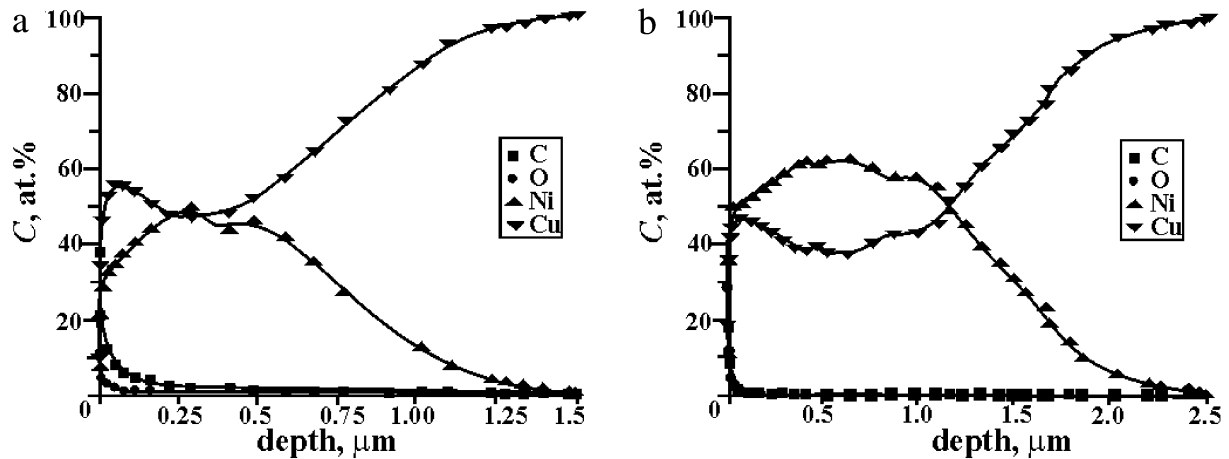
Fig. 19. AES depth profiles of elements for system Ni (coating)–Cu (substrate) irradiated with LEHCEB: (a) Ni (3 μm; 2.5 μS, 4 J/cm^2, $N = 30$); (b) Ni (5 μm; 2.5 μS, 9 J/cm^2, $N = 15$) followed by Ni (5 μm; 2.5 μS, 9 J/cm^2, $N = 30$).

If an auxiliary target (e.g., a grid) is placed in front of the surface under irradiation, it is possible to execute evaporation of the target, transfer of the target material in the form of vapors and ions to the surface, and pulsed melting of the surface layer (Proskurovsky *et al.*, 1997). The concentration of alloying elements and the thickness of the alloyed layer can be gradually increased by increasing the number of irradiation cycles. Figure 20 shows the concentration profiles obtained by the AES method for samples of Armco iron alloyed with Al. It can be seen that a layer ~4 μm thick has been formed on the surface which contained, in fact, 100% Al. Then a transitory layer ~4 μm thick follows with the Al concentration gradually decreasing to zero. The results obtained suggest that LEHCEB sources hold promise for producing highly alloyed surface layers, including layers of intermetallic compounds (based on systems of Fe-Al, Ti-Al, Ni-Al, and the like).
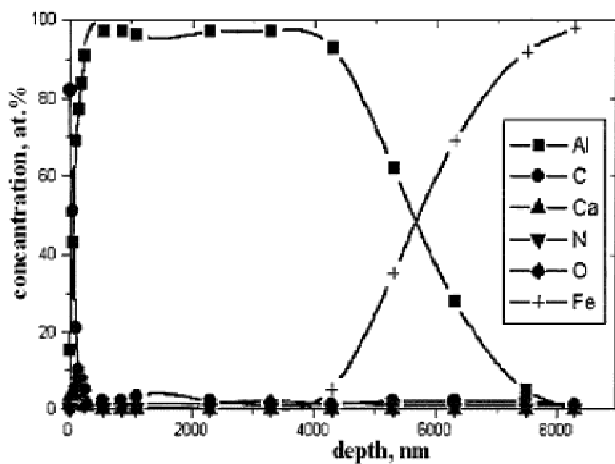

Fig. 20. AES depth profiles of elements for Armco-Fe samples after electron beam surface alloying with Al.

7.2.6. Surface treatment of dental alloys

Experiments (Raharjo *et al.*, 2002) were performed to investigate the effect of pulsed melting on the surface morphology and properties of metal casting dentures. The need in these investigations was conditioned by the fact that the conventional methods for cleaning and smoothing of the surface of dentures, including grinding and mechanical polishing, are labor intensive and not very productive. Most of the experiments were performed with samples and dentures made of standard dental materials: commercial titanium and Ti-6Al-4V and 61Co-31Cr-6Mo alloys. For Ti and the Ti alloy, prior to irradiation, the surface was chemically etched to remove the oxide layer (80–100 μm) formed after casting. For the Co-Cr-Mo alloy, in some experiments, the original (after casting) surface was coated with Ti by the PDV method. Electron-beam treatment was performed on a specially designed automated electron-beam setup based on an LEHCEB source, which was furnished with a manipulator that allowed 12 dentures to be treated in one vacuum cycle.

It has been established that for titanium, the presence of the residues of the oxide layer not completely removed by chemical etching gives rise to microtracking of the irradiated surface. Obviously, this is related to the high embrittlement of the titanium oxide. If the oxide layer is removed completely, there are no microcracks on the irradiated surface. In optimum treatment modes, the surface roughness R_a decreases to 0.27 μm (compared to 1.62 μm in the original state) and the coefficient of reflection almost doubles. Measurements of the anode polarization characteristics in the solution 1N HCl have shown that, after irradiation, the current density decreased to one-third of its original value. The increase in corrosion resistance correlates well with the smoothing of the surface and with its cleaning of oxygen and carbon impurities, detected earlier (Nochovnaya *et al.*, 1998; Proskurovsky *et al.*, 1998).

When the Co-Cr-Mo alloy was subjected to irradiation, microcraters formed on its surface, and, in contrast to titanium alloys and stainless steels, crater formation could not be suppressed even by multiply repeated pulsed melting. However, if Ti film was previously deposited on the surface, irradiation in a proper mode made it possible to substantially reduce the microcrater density and obtain a high-quality surface (Fig. 21). Since Co and Cr show comparatively low solvability in α-Ti (in contrast to Mo), the liquid-phase mixing may give rise to the formation a Ti-based surface alloy containing the substrate components.

The results obtained, in view of the large cross section of the beam and the high productivity of the electron-beam setup, can be considered a basis for the development of a new technology for surface modification of dental materials. On the other hand, since Ti-based alloys and Co-Cr-Mo alloys are the principal metallic biomaterials (Jones, 2001), these methods may appear to be highly promising for improving corrosion resistance and biocompatibility of biomedical implants (components of hip and knee joints, dentures, etc.). In addition, the data reported by Nochovnaya *et al.* (1998) and Proskurovsky *et al.* (1998) suggest that there exists the possibility to increase the fatigue strength of implants made of titanium alloys.

8. DESCRIPTION OF THE LEHCEB SOURCE

As an example, we give a description of a recent version of the LEHCEB source. The main component of the source is a gun with a plasma anode based on a high-current (150 A) reflected discharge in argon. The explosive-emission cathode of 7 or 9 cm diameter is made of copper or titanium multiwire plexus pressed in a ring made of type 12X18H10T stainless steel. The discharge anode is a ring of 8–10 cm internal diameter and 2–4 cm in length. An external guide magnetic field of strength up to 2 kOe is created by Helmholtz coils powered from a capacitor bank. The electron gun is butt-jointed with the working chamber, which is furnished with a manipulator to revolve the articles under treatment.

The high-voltage pulse generator is constructed based on a type IK-50/3 capacitor (50 kV, 3 μF) and a type TDI1-50k/50 pseudospark switch. The series inductance and impedance were, respectively, 200 nH and 0.25 Ω, respectively. The generator is connected with the electron gun by a transmission line made of six parallel pieces of 50-Ω coaxial cable, each about 1 m long.

The working chamber is evacuated with a turbo-molecular pump to a pressure of 10^{-6} Torr. The working gas is supplied in a steady mode. The transition of the reflected discharge into its high-current stage is provided due to the long duration of the pulsed voltage applied to the discharge anode (about 800 μs).

The following beam parameters have been attained: average electron energy 12–15 keV, beam current up to 30 kA, pulse duration 2–4 μs, pulse repetition rate 0.1–0.2 Hz, beam diameter up to 11 cm, energy density up to 15 J/cm^2, and cross-sectional beam nonuniformity 15–20%. The key components of the LEHCEB sources that are responsible for its operability are the explosive-emission cathode and the VPG. Our experience of operating LEHCEB sources has shown that the lifetime of the cathode depends mainly on the vacuum conditions. For the operation under vacuum conditions provided by an oil-vapor diffusion pump, the cathode lifetime achieved by now is over 10^5 pulses, and it can further be increased. A similar result has been obtained when the chamber was evacuated by a turbo-molecular pump to pressures of 5×10^{-5}–10^{-4} Torr. However, in experiments on increasing the electric strength of vacuum insulation where a turbo-molecular pump evacuated the chamber to 10^{-6} Torr and the cathode was substantially dusted with stainless steel, the cathode lifetime was significantly shorter (1,500 pulses). The criterion for failure served the 3% probability of the beam generation ceasing. However, in view of the low cost of the cathode and the opportunity of its quick replacement, this lifetime can be considered satisfactory.

The main components of the VPG have stood up to a total of about 70,000 pulses, often operated continuously at a frequency of 0.2 Hz for 8 h. These results suggest that the VPG is reliable enough for technological applications.
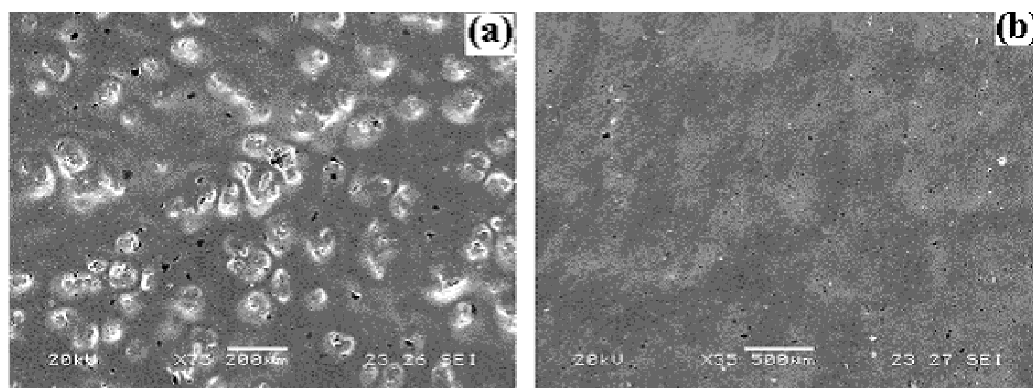

Fig. 21. SEM images of a surface of CoCrMo alloy irradiated with LEHCEB: without (a) and with (b) Ti precoating.

One LEHCEB source has been used, since April, 2001, in the Niigata Laboratory of ITAC Ltd. (Japan) in developing a technology for finish cleaning and smoothing of dentures.

9. CONCLUSION

The results of the investigations and tests performed make it possible to develop pilot-plant systems for pulsed electron-beam treatment of materials. The reliability of LEHCEB sources of this type and their comparatively low cost are ensured by the moderate parameters of the high-voltage pulses used that are responsible for the appropriate lifetimes of key power supply circuit components (pulsed capacitors, spark gap switches). A system intended for finish treatment of dentures produced in 2001 jointly with ITAC Ltd. (Japan) is currently used to advantage.

Further development of LEHCEB sources is associated with widening the ranges of the beam parameters (first of all, increasing the pulse duration), increasing the efficiency of conversion of the energy stored in the high-voltage pulse generator to the beam energy, and lengthening the lifetime of the cathode operated in oil-free vacuum. We attach particular significance to refining the methods of the formation of a plasma anode, and primarily to improving the uniformity of the cross-sectional ion current density distribution.

The characteristics and mechanisms for the modification of the microstructure and properties of the surface layers of materials irradiated by LEHCEBs are also discussed. The results obtained suggest that LEHCEBs are promising for the development of new methods of surface treatment of materials. For some applications, such as medical ones, of considerable interest might be the surface alloying methods based on liquid-phase mixing of the components of film–substrate systems.

ACKNOWLEDGMENTS

REFERENCES

ARZHANNIKOV, A.V., BURDAKOV, A.V., DEICHULI, P.P., KOIDAN, V.S., KONYUKHOV, V.V. & MEKLER, K.I. (1978). Measurement of the parameters of the pulsed high voltage Penning discharge plasma with the use of double probe. *Sov. J. Plasma Phys.* **4**, 1133–1140.

ARZHANNIKOV, A.V., BURMASOV, V.S., VYACHESLAVOV, L.N. & KOIDAN, V.S. (1984). Production of a dense plasma column in a strong magnetic field and its diagnostics with laser technique. *Sov. J. Plasma Phys.* **10**, 175–182.

BABERTSYAN, R.P., BADALYAN, E.S., EGIAZARYAN, G.A. & TER-GEVORKYAN, E.S. (2000). Influence of the electrodes geometry on characteristics of the Penning discharge. *Sov. Phys. Tech. Phys.* **70**, 24–28.

BARDENSHTEIN, A.L., BUSHNEV, L.S., DUDAREV, E.F., MARKOV, A.B. & ROTSHTEIN, V.P. (2000). Thermal stresses and twinning in thin copper samples irradiated with high-current electron beam. In *Proc. 5th Int. Conf. on Modification of Materials with Particle Beams and Plasma Flows*. (Mesyats, G.A., Bugaev S.P. & Ryabchikov A.I., Eds.), pp. 43–47.

BATRAKOV, A.V., KARLIK, K.V., KITSANOV, S.A., KLIMOV, A.I., KONOVALOV, I.N., KOROVIN, S.D., MESYATS, G.A., OZUR, G.E., PEGEL', I.V., POLEVIN, S.D., PROSKUROVSKY, D.I. & SUKHOV, M.YU. (2001). Relativistic gigawatt BWO microwave pulse duration increase upon treating the slow-wave structure surface with a low-energy high-current electron beam. *Tech. Phys. Let.* **27**, 150–152.

BATRAKOV, A.V., MARKOV, A.B., OZUR, G.E., PROSKUROVSKY, D.I. & ROTSHTEIN, V.P. (1995). The effect of pulsed electron-beam treatment of electrodes on vacuum breakdown. *IEEE Trans. on Dielectric and Electric Insul.* **2**, 237–242.

BOLEY, B.A. & WEINER, J. (1960). *Theory of Thermal Stresses*. New York: Wiley.

BUGAEV, S.P., KIM, A.A., KOSHELEV, V.I. & KHRYAPOV, P.A. (1982). Cathaode plasma movement across the uniform magnetic field in the diodes with explosive emission. *Bull. Acad. Sci. USSR Phys. Ser.*, **46**, 1300–1305.

DUDAREV, E.F., POCHIVALOVA, G.P., PROSKUROVSKY, D.I., ROTSHTEIN, V.P. & MARKOV, A.B. (1996). Microplastic deformation of Fe and Mo polycrystals irradiated with low-energy, high-current electron beam. *Izv. Vyssh. Uchebn. Zaved. Fiz.*, No. 3, 126–132.

GNYUSOV, S.F., TARASOV, S.YU., IVANOV. YU.F. & ROTSHTEIN, V.P. (2002). Influence of the pulsed electron-beam melting on microstructure and tribo-technical characteristics of WC-steel 110G13 hard alloy. In *Proc. 6th Int. Conf. on Modification of Materials with Particle Beams and Plasma Flows*. (Mesyats G.A., Korovin S.D. & Ryabchikov, A.I., Eds.), pp. 277–283.

IGNATOV, A.M. & RUKHADZE, A.A. (1984). To the theory of Pierce instability of neutralized electron beams. *Sov. J. Plasma Phys.* **10**, 112–114.

IREMASHVILI, D.V., OSEPASHVILI, T.A. & KAKUCHAYA, P.I. (1975). Formation of the high intensive microsecond electron beams. *Sov. Tech. Phys. Lett.* **1**, 508–511.

IVANOV, YU.F., ITIN, V.I., LYKOV, S.V., MARKOV, A.B., ROTSHTEIN, V.P, TUHFATULLIN, A.A. & DIKIY, N.P. (1993).Structural analysis of heat affected zone of steel 45 treated with low-energy high-current electron beam. *Fizika metallov i metallovedenie* **75**, 103–112.

IVANOV, YU.F., KRYUCHKOV, YU.YU., MARKOV, A.B., NAZAROV, D.S., OZUR, G.E., POGREBNYAK, A.D., PROSKUROVSKY, D.I. & ROTSHTEIN, V.P. (1994). Pulsed electron-beam mixing of Ta-Fe system. *Poverhnost'* No. 10–11, 95–102.

IVANOV, YU.F., MATZ, W., ROTSHTEIN, V.P., GUENZEL, R. & SHEVCHENKO, N.A. (2002). Pulsed electron-beam melting of high-speed steel: Structural phase transformations and wear resistance. *Surf. Coat. Technol*. **150**, 188–198.

IVANOV, YU.F., ROTSHTEIN, V.P., PROSKUROVSKY, D.I., ORLOV, P.V., POLESTCHENKO, K.N., OZUR, G.E. & GONCHARENKO, I.M. (2000). Pulsed electron-beam treatment of WC-TiC-Co hard-alloy cutting tools: Wear resistance and microstructural evolution. *Surf. Coat. Technol.* **125**, 251–256.

JONES, F.H. (2001). Teeth and bones: Applications of surface science to dental materials and related biomaterials. *Surf. Sci. Rep.* **42**, 75–205.

KARLIK, K.V., MYAGKOV, A.S., OZUR, G.E. & PROSKUROVSKY, D.I. (2002). Investigations of the plasma generator based on low pressure, high current reflected discharge. In *Proc. 6th Int. Conf. on Modification of Materials with Particle Beams and Plasma Flows* (Mesyats, G.A., Korovin, S.D. & Ryabchikov, A.I., Eds.), pp. 96–99.

KOROVIN, S.D., MESYATS, G.A., PEGEL', I.V., POLEVIN, S.D. & TARAKANOV, V.P. (2000). Mechanism of microwave pulse shortening in the relativistic backward wave oscillator. *IEEE Trans. Plasma Sci.* **28**, 485–495.

KRASTELEV, E.G., AGAFONOV, A.V. & MIKHALEV, P.S. (2000). A high-current non-relativistic electron beam generation in a diode with column-like plasma anode. In *Proc. 12th Symp. on High Current Electronics* (Mesyats, G.A., Kovalchuk, B.M. & Remnev, G.E., Eds.), pp. 119–120.

KREINDEL', M.YU., LITVINOV, E.A., OZUR, G.E. & PROSKUROVSKY, D.I. (1991). Non-stationary processes in initial stage of the high-current electron beam formation in a plasma-filled diode. *Sov. J. Plasma Phys.* **17**, 1425–1439.

KREINDEL', YU.E. (1977). *Plasma Sources of Electrons*. Moscow: Atomizdat.

LEBEDEV, P.M., ONISHCHENKO, I.N., TKACH, YU.V., FAINBERG, YA.B. & SHEVCHENKO, V.I. (1976). The theory of the beam-plasma discharge. *Sov. J. Plasma Phys.* **2**, 407–413.

LUTSENKO, E.I., SEREDA, N.D. & KONTSEVOI, L.M. (1976). Investigation of space charge layers formation in plasma. *Sov. J. Plasma Phys.* **2**, 72–81.

LUTSENKO, E.I., SEREDA, N.D. & TSELUIKO, A.F. (1988). Dynamic double layers in high current plasma diodes. *Sov. Phys. Tech. Phys.* **58**, 1299–1309.

LUTZ, M.A. (1974). The glow to arc transition—A critical review. *IEEE Trans. Plasma Sci.* **2**, 1–10.

MARKOV, A.B., IVANOV, YU.F., PROSKUROVSKY, D.I. & ROTSHTEIN, V.P. (1999). Mechanisms for hardening of carbon steel with nanosecond high-energy, high-current electron beam. *Mater. Manuf. Processes* **14**, 205–216.

MARKOV, A.B. & ROTSHTEIN, V.P. (1997). Calculation and experimental determination of dimensions of hardening and tempering zones on quenched U7A steel irradiated with a pulsed electron beam. *Nucl. Instrum. Methods B* **132**, 79–86.

MESYATS, G.A. & PROSKUROVSKY, D.I. (1989). *Pulsed Electrical Discharge in Vacuum*. Germany: Springer-Verlag.

NAZAROV, D.S., OZUR, G.E. & PROSKUROVSKY, D.I. (1994). Generation of low-energy, high-current electron beams in a gun with plasma anode. *Sov. Phys. J.* No. 3, 100–114.

NAZAROV, D.S., OZUR, G.E. & PROSKUROVSKY, D.I. (1995). Energy losses of low-energy, high-current electron beam under transportation through rarefied plasma. *Sov. J. Plasma Phys.* **21**, 173–179.

NAZAROV, D.S., OZUR, G.E. & PROSKUROVSKY, D.I. (1996). A source of high-density pulsed electron beams with energies up to 40 keV. *Instrum. Exp. Tech.* **39**, No. 4, 546–551.

NAZAROV, D.S., OZUR G.E. & PROSKUROVSKY, D.I. (1997). Production of low-energy, high-current electron beams in a reflected-discharge plasma-anode gun. In *Proc. 11th IEEE Int. Pulsed Power Conf.* vol. 2, pp. 1335–1340.

NEZLIN, M.V. (1982). *Dynamics of Beams in Plasma*. Moscow: Energoatomizdat.

NOCHOVNAYA, N.A., SHULOV, V.A., NAZAROV, D.S., OZUR, G.E., PROSKUROVSKY, D.I., ROTSHTEIN, V.P. & KARPOVA, I.G. (1998). Treatment of parts made of titanium alloys with low-energy, high-current electron beams of microsecond duration. *Fizika i Hiniya Obrabotki Materialov* No. 1, 27–33.

OZUR, G.E., MYAGKOV, A.S. & PROSKUROVSKY, D.I. (2000a). Transportation of a low-energy, high-current electron beam in a long plasma channel. In *Proc. 12th Symp. on High Current Electronics* (Mesyats, G.A., Kovalchuk, B.M. & Remnev, G.E., Eds.), pp. 115–117.

OZUR, G.E. & PROSKUROVSKY, D.I. (1989). Measuring parameters of plasma generated by multi-point vacuum arc. In *Proc. 11th All-Union Conf. on Generators of Low-Temperature Plasma* vol. 1, pp. 143–144.

OZUR, G.E. & PROSKUROVSKY, D.I. (1990). Generation of low-energy, high-current electron beam in the diode with plasma anode. *Proc. 14th Int. Symp. on Discharges and Electrical Insulation in Vacuum* pp. 665–670.

OZUR, G.E., PROSKUROVSKY, D.I. & KARLIK, K.V. (2000b). Pulsed electron beam system for material surface treatment. In *Proc. 5th Conf. on Modification of Materials with Particle Beams and Plasma Flows* (Mesyats, G.A., Bugaev, S.P. & Ryabchikov, A., Eds.), pp. 139–142.

PERRY, A., MATOSSIAN, J., BULL, S., PROSKUROVSKY, D.I., RICE-EVANS, P., PAGE, T., GEINST, D., TAYLOR, J., VAJO, J., DOTTY, R., ROTSHTEIN, V.P. & MARKOV, A.B. (1999). Rapid thermal processing of TiN coatings deposited by chemical and physical vapor deposition using a low-energy, high-current electron beam: Microstructural studies and properties. *Metall. Mater. Trans. A* **30**, 2931–2939.

PFEIL, P.C.L. & GRIFFITHS, L.B. (1959). Dielectric inclusions influence on arc initiation. *J. Nucl. Mater.*, **3**, 244–248.

PLYUTTO, A.A., SULADZE, K.V., TEMCHIN, S.M. & KOROP, E.D. (1969). Intensive electron beams formation in confined plasma. *Sov. At. Energy*, **27**, 418–420.

POATE, J.M., FOTI, G. & JACOBSON, D.S., EDS. (1983). *Surface Modification and Alloying by Laser, Ion, and Electron Beams*. New York: Plenum Press.

PROSKUROVSKY, D.I. (2002). Surface treatment of electrodes by intense flows of charged particles as the method for improvement of vacuum insulation. In *Proc. 20th Int. Symp. on Discharges & Electrical Insulation in Vacuum*, pp. 147–153.

PROSKUROVSKY, D.I., ROTSHTEIN, V.P. & OZUR, G.E. (1996). Application of low-energy, high-current electron beams for surface modification of materials. *Proc. 11th Int. Conf. on High Power Particle Beams (BEAMS-96)* (Jungwirth, K. & Ullschmied, J., Eds.), vol. I, pp. 259–262.

PROSKUROVSKY, D.I., ROTSHTEIN, V.P. & OZUR, G.E. (1997). Use of low-energy, high-current electron beams for surface treatment of materials. *Surf. Coat. Technol.* **96**, 117–122.

PROSKUROVSKY, D.I., ROTSHTEIN, V.P., OZUR, G.E., IVANOV, YU.F. & MARKOV, A.B. (2000). Physical foundations for surface treatment of materials with low energy, high current electron beams. *Surf. Coat. Technol.* **125**, 49–56.

PROSKUROVSKY, D.I., ROTSHTEIN, V.P., OZUR, G.E., MARKOV, A.B., NAZAROV, D.S., IVANOV, YU.F., SHULOV, V.A. & BUCHHEIT, R.G. (1998). Pulsed electron-beam technology for surface modification of metallic materials. *J. Vac. Sci. Technol.* **A16**, 2480–2488.

RAHARJO, P., WADA, H., NOMURA, Y., OZUR, G.E., PROSKUROVSKY, D.I., ROTSHTEIN, V.P. & UEMURA, K. (2002). Pulsed

electron beam technology for surface modification of dental materials. In *Proc. 6th Int. Conf. on Modification of Materials with Particle Beams and Plasma Flows* (Mesyats, G.A., Korovin, S.D. & Ryabchikov, A.I., Eds.), pp. 679–692.

ROTSHTEIN, V.P., IVANOV, YU.F., PROSKUROVSKY, D.I., KARLIK, K.V., SHULEPOV, I.A. & POCHIVALOVA, G.P. (2002). Microstructure of the near-surface layers of austenitic stainless steels irradiated with low-energy high-current electron beam. In *Proc.*

6th Int. Conf. on Modification of Materials with Particle Beams and Plasma Flows (Mesyats, G.A., Korovin, S.D. & Ryabchikov, A.I., Eds.), pp. 205–210.

VYBORNOV, S.I., ZHARINOV, A.V. & MALAFAEV, V.A. (1988). A periodic Pierce instability and limiting currents of electron beams with the arbitrary degree of the space charge neutralization in the transportation channel. *Sov. J. Plasma Phys.*, **14**, 84–90.